Localized-itinerant electronic transition in the perovskite system $La_{1-x}Ca_xVO_3$

Hoan C. Nguyen and John B. Goodenough
Center for Materials Science and Engineering, ETC 9.102, The University of Texas at Austin, Austin, Texas 78712-1063
(Received 28 March 1995)

The insulator-metal (*I-M*) transition near the critical composition $x_c \approx 0.26$ in $La_{1-x}Ca_xVO_3$ is confirmed, as is the apparent existence of a solid solution over the entire compositional range $0 \le x \le 1$ according to room-temperature powder x-ray diffraction. Although interpretation of the evolution with x of its physical properties would seem to require a global electronic model, the magnetic and transport properties we measure below room temperature suggest the presence of a two-phase electronic model with itinerant-electron behavior in hole-rich (or electron-poor) domains and localized-electron behavior in hole-poor domains. Localized electronic states within the itinerant-electron domains are associated with atomic vacancies or lattice defects. The system may remain atomically disordered, but an electronic phase segregation can be accomplished at lower temperatures by cooperative oxygen-atom displacements. Separation into electronically distinguishable phases by this mechanism would not be detected easily by powder x-ray diffraction. A first-order structural phase transition occurs in the interval 400–640 K for all x; the high-temperature phase exhibits a Curie-Weiss paramagnetism.

INTRODUCTION

It has been recognized for many years now that transition-metal oxides with a perovskite structure offer the opportunity to study the transition from localized-electron to itinerant-electron behavior in systems where nearly 180° metal-oxygen-metal (*M-O-M*) interactions are dominant.[1] Initial experiments concentrated on single-valent perovskites; however, it was recognized that oxygen nonstoichiometry could profoundly influence the Coulombic interactions between the electrons of interest.[2] Recently cuprate superconductors have highlighted the need for better descriptions of the transformation from localized to itinerant electronic behavior in mixed-valent perovskite-related systems, particularly those where a parent compound is an antiferromagnetic spin-$\frac{1}{2}$ insulator. In this paper we report a measurement of the nominal $La_{1-x}Ca_xVO_3$ system over the entire compositional range $0 \le x \le 1$. Our data and interpretation are to be compared with a similar study made for $0 \le x \le 0.5$,[3] and reports[4–6] on the sister systems $La_{1-x}Sr_xVO_3$ and $Y_{1-x}Ca_xVO_3$.

An AMO_3 perovskite contains an MO_3 array of corner-shared MO_6 octahedra. We emphasize three features. First, by changing the mean valence state of the A cation, it is possible to vary continuously the oxidation state of the MO_3 array without changing the oxygen coordination at a transition-metal atom M. Second, the strength of the *M-O-M* interactions of an MO_3 array depend on the *M-O-M* bond-angle and bond-length mismatch; they may be varied not only by changing the oxidation state of the MO_3 array, but also by changing the ionic radius of the A cation without changing its valence state.[7] Third, displacement of an oxygen atom toward one of its two M-atoms near neighbors and away from the other is possible without changing significantly the *M-M* separation, i.e., the lattice parameter. Cooperative oxygen displacements can separate domains of shorter and longer mean M—O bond length either in the formation of a small polaron or of an M-atom cluster of shorter mean M—O bond length about a substitutional A cation. Near a transition from localized to itinerant electronic behavior, trapping of holes in the domains of shorter mean M—O bond length can create an electronic phase segregation within an atomic solid-solution range since we can expect the electronic behaviors of the itinerant and localized electrons to be distinguishable. We have used magnetic and transport measurements to investigate whether there is evidence of an electronic phase segregation below room temperature in the mixed-valent, orthorhombic system $La_{1-x}Ca_xVO_3$.

We also call attention to the Virial theorem

$$2\langle T\rangle + \langle V\rangle = 0 , \tag{1}$$

which states that a discontinuous change in the mean kinetic energy $\langle T\rangle$ of the electrons of an MO_3 array must be compensated for by a discontinuous change in the mean potential energy $\langle V\rangle$, and a discontinuous change $\Delta\langle V\rangle$ would be reflected in the mean equilibrium M—O bond length. The more localized the antibonding, primarily M $3d$ electrons of an MO_3 array, the longer should be the mean equilibrium M—O bond length. It follows that we can expect to find strong electron-lattice interactions at any transition from more localized to more extended electronic states that involves a discontinuous change in the mean electron kinetic energy $\langle T\rangle$.

In single-valent systems, we may anticipate a discontinuous change $\Delta\langle T\rangle$ on passing from a localized-electron to an itinerant-electron configuration, which implies a discontinuous volume change and hence a first-order transition. In a mixed-valent system, strong electron-lattice interactions can be expected to result in either the formation of nonadiabatic polarons or phase segregation. A transition from polaronic to itinerant-electron behavior may also result in discontinuous contraction of the VO_3 array.

We shall apply these principles to our interpretation of the data we report for the nominal system $La_{1-x}Ca_xVO_3$ with $0 \leq x \leq 1$.

PREVIOUS WORK

The $LnVO_3$ family, where Ln is a trivalent rare-earth cation, illustrates a first-order transition with decreasing V—O bond length from localized-electron to itinerant-electron antiferromagnetism in a single-valent $(VO_3)^{3-}$ array. $LaVO_3$ is an antiferromagnetic insulator with a localized V^{3+}: $^3T_{1g}$ ground-state configuration having an orbital angular momentum that is not completely quenched ($M_L = 0, \pm 1$) in a cubic crystalline field. Below an antiferromagnetic Néel temperature $T_N \approx 142$ K,[8] the spins are canted to give a weak ferromagnetism.[9,10] Ordering of the spins below T_N allows the spin-orbit coupling to order the electrons into orbitals ordered with respect to the spin directions so as to produce a cooperative magnetostrictive distortion below a $T_t \approx 138$ K $< T_N$ that stabilizes the $M_L = \pm 1$ state relative to the $M_L = 0$ state; spin-orbit coupling removes the remaining orbital degeneracy.[11] We have shown elsewhere[12,13] that the direction of the vanadium atomic moment μ_v is reversed on thermally traversing the temperature T_t. This phenomenon is responsible for the anomalous diamagnetism that was reported[14,15] for field-cooled (in 1 kOe) $LaVO_3$.

Preparation of $LaVO_3$ and cooling to room temperature under a hydrostatic pressure $P > 8$ kbar gives an orthorhombic phase of the same *Pbnm* space group, but with a somewhat smaller volume.[13] The metastable high-pressure phase has a T_N that is changed little from that of the stable atmospheric-pressure phase, but it exhibits neither a weak ferromagnetism below T_N nor a magnetostrictive distortion below a $T_t < T_N$. The high-pressure metastable phase undergoes a first-order transition back to the stable phase on heating to above 250 °C. The first-order character of the transition from localized-electron to itinerant-electron antiferromagnetism is also manifest as a miscibility gap in the $La_{1-x}Y_xVO_3$ system even though $LaVO_3$ and YVO_3 are isostructural. The smaller size of the Y^{3+} ion introduces a mismatch between the Y—O and V—O bond lengths that places the $(VO_3)^{3-}$ array under a greater compressive stress; introduction of the smaller Y^{3+} ion represents a chemical application of hydrostatic pressure.

In an early study, Reuter and Wollnik[16] reported that the system $La_{1-x}Ca_xVO_3$ forms a solid solution over the entire compositional range $0 \leq x \leq 1$. Dougier, Deglane, and Hagenmuller[3] explored the single-phase region over the range $0 \leq x \leq 0.5$. They also made magnetic-susceptibility, resistivity, and thermoelectric power measurements on polycrystalline samples from 77 to 600 K. They reported an insulator-metal transition occurring within the single-phase domain near $x \approx 0.26$ and interpreted it as an Anderson transition, the Fermi energy E_F dropping across a mobility edge in the lower-π^* Hubbard band, which corresponds to the V^{4+}/V^{3+} couple, at the composition $x_c \approx 0.26$.

On the other side of the phase diagram, the end member $CaVO_3$ has been variously reported to be Pauli paramagnetic,[17] antiferromagnetic ($T_N \approx 170$, K),[18] and Curie-Weiss paramagnetic with no magnetic order down to 4 K.[19] These differences reflect problems with oxygen stoichiometry. The sample showing Curie-Weiss paramagnetism with no long-range magnetic order was an as-grown single crystal that was oxygen deficient. After an anneal in air at 450 K for 24 h, it became oxygen-stoichiometric $CaVO_3$. The stoichiometric single crystal had a small resistance and was Pauli paramagnetic; its electrical resistivity followed a $\rho = \rho_0 + AT^2$ relation over a wide temperature range typical of a strongly correlated, narrow conduction band; and it showed a positive magnetoresistance that varies as the square of the magnetic field (B^2). At least some V $3d$ electrons of $CaVO_3$ are itinerant.

Kasuya *et al.*[6] studied the system $Y_{1-x}Ca_xVO_3$; they found, from room-temperature x-ray powder diffraction, a smooth variation of orthorhombic lattice parameters over the entire compositional range $0 \leq x \leq 1$ and an insulator-metal (*I-M*) transition at $x \approx 0.5$. With increasing x, a mid-infrared-absorption band was found to grow in intensity in the insulator range $0 < x \leq 0.5$ and to merge increasingly with a Drude-like response in the metallic region on the approach to $CaVO_3$ ($x = 1$). They assumed a complete solid solution over the range $0 \leq x \leq 1$ and accordingly interpreted their data within a global

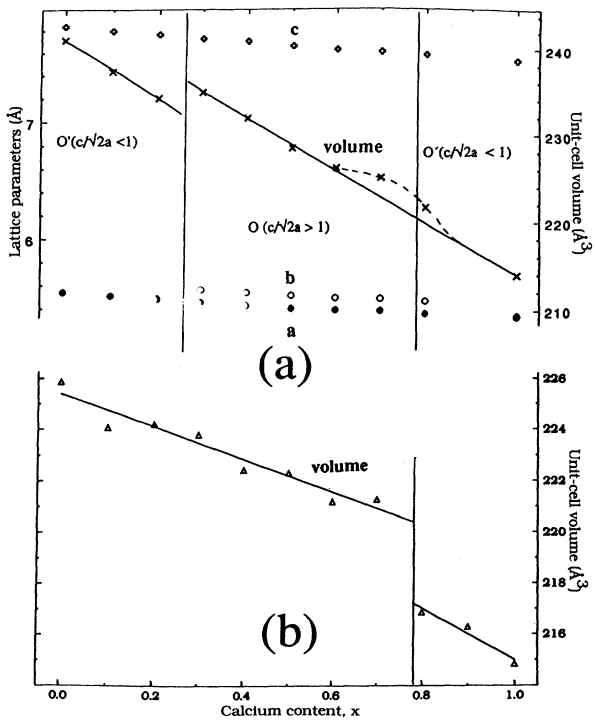

FIG. 1. (a) Variation with x of orthorhombic lattice parameters and unit-cell volume (×) for $La_{1-x}Ca_xVO_{3\pm\delta}$. (b) Variation with x of unit-cell volume (△) of $Y_{1-x}Ca_xVO_3$ as calculated from Ref. 6. Solid lines are drawn as guides to the eye for Végard's law; the dashed line shows the deviation from Végard's law.

model of the electronic system in which the electron correlations evolve uniformly with x. On the other hand, they recognized that their optical data indicate a transfer of spectral weight, increasing with x, from the upper and lower Hubband bands (the empty $V^{3+}/V^{2+}:t^3e^0$ and filled $V^{4+}/V^{3+}:t^2e^0$ redox couples in the strongly correlated antiferromagnetic end member YVO_3) to near the Fermi energy in the energy gap between them. Since the structural data show an axial c/a ratio dropping much more steeply with increasing x on the metallic side of the *I-M* transition in the range $0.5<x<0.8$, we calculated from their data the evolution of the unit-cell volume with x; the resulting plot (see Fig. 1) shows two ranges of x in which the unit-cell volume varies linearly with x, obeying Végard's law, but with a discontinuity between them at $x\approx 0.75$.

For the sister system $La_{1-x}Sr_xVO_3$, Dougier and Hagenmuller[4] reported a smooth semiconductor-metal (*I-M*) transition at $x_c\approx 0.225$. The antiferromagnetic Néel temperature T_N falls monotonically from 142 K at $x=0$ to 100 K near $x=0.2$, then drops abruptly to 0 K at x_c. Mahajan *et al.*[5] reinvestigated the system and reported a complete solid solubility over the compositional range $0\le x\le 1$, the lattice parameter varying linearly with x according to Végard's law. They confirmed the transition from an antiferromagnetic insulator to a metallic, strongly exchange-enhanced Pauli paramagnetic metal at an $x_c\approx 0.2$. The room-temperature magnetic susceptibility varies smoothly with x through x_c, and the magnetic susceptibility is temperature independent for all $x>x_c$. Nevertheless the magnitude of the Pauli paramagnetism and ^{51}V NMR data shows a strong enhancement of the Stoner type as well as a mass enhancement. Unlike the situation in the superconductive cuprates, they found no evidence for antiferromagnetic-spin fluctuations at room temperature in their metallic samples. Mott *et al.*[20] suggested that the semiconductor-metal transition represents a crossing of a mobility edge by E_F in the lower Hubbard band; but this interpretation is not supported by high-resolution photoemission spectroscopy (PES) measurements,[21] which found an increase in the width of the π^* band of the VO_3 array on increasing x across x_c and no density of states at E_F for $x<x_c$. In $La_{1-x}Sr_xVO_3$ there is no evidence of an electronic phase segregation at room temperature.

Dougier, Fan, and Goodenough[2] reported that stoichiometric $SrVO_3$, which is cubic and exhibits a ferromagnetic spin-density wave below 85 K, is metallic with respect to a first-order loss of oxygen to orthorhombic $SrVO_{2.9}$, which remains Pauli paramagnetic to lowest temperatures.

EXPERIMENTAL PROCEDURES

$LaVO_4$ and $Ca_2V_2O_7$ were first prepared by standard solid-state reaction of stoichiometry mixtures of dried La_2O_3, $CaCO_3$, and V_2O_5 powders in air at 850 °C. Next, the end members $LaVO_3$ and $CaVO_3$ were made by reducing $LaVO_4$ and $Ca_2V_2O_7$ in flowing hydrogen at 1100 and 800 °C, respectively. Finally, polycrystalline $La_{1-x}Ca_xVO_3$ compounds were made from appropriate mixtures of $LaVO_3$ and $CaVO_3$ by solid-state reaction at 1400 °C in ultrapure argon with several intermittent regrindings.

All samples investigated contained only the perovskite phase to x-ray powder diffraction taken with a Philips diffractometer and Cu $K\alpha$ radiation; Si was used as an internal standard to calibrate the peak positions. Lattice parameters were obtained with a least-squares fitting procedure.

A Perkin-Elmer TGA-7 thermogravimetric analyzer (TGA) was used to determine the oxygen content of our samples from the weight gain on oxidation of the vanadium ions to V^{5+} on heating to 700 °C in dried air. A Perkin-Elmer DSC-7 differential scanning calorimeter was measured in nitrogen atmosphere up to 600 °C to obtain a phase transition.

Magnetic susceptibilities were obtained between 5 and 800 K in a field of 1 kOe with a superconducting quantum interference device (SQUID) magnetometer. Four-probe dc resistance measurements made on polycrystalline discs were corrected for the thermoelectric contribution by subtraction of the off-current background. The dc thermoelectric power was measured with a home-built experimental system, described elsewhere,[22] to obtain the Seebeck coefficient from 15 to 310 K; the temperature difference across the sample in each measurement rose to 5 K.

RESULTS

(1) *X-ray diffraction and TGA:* Lattice parameters and unit-cell volumes obtained from powder x-ray diffraction for the orthorhombic (*Pbnm*) system $La_{1-x}Ca_xVO_3$ indicate a complete solid solution over the range $0\le x\le 1$, but with what appears to be a small discontinuous break in the evolution of volume with x in the range $0.2<x<0.3$ (see Fig. 1), where Dougier, Deglane, and Hagenmuller[3] reported an insulator-metal (*I-M*) transition. We note a change in the room-temperature orthorhombic (*Pbnm*) axial ratio from $c/\sqrt{2}a<1$ to $c/\sqrt{2}a>1$, i.e., from the *O'* to the *O* orthorhombic structure as distinguished in Ref. 7, in the interval

TABLE I. Variation with doping concentration x in $La_{1-x}Ca_xVO_3$, with $0\le x\le 1$ of room-temperature lattice parameters, oxygen content, critical temperatures T_{sg}, T_N, T_t, T^*, and μ_{eff} evaluated from the molar susceptibility at $T>640$ K.

$x=$	a (Å)	b (Å)	c (Å)	$3+\delta$	μ_{eff}	T_{sg} (K)	T_N or T^* (K)	T_t
0.0	5.547	5.546	7.842	3.01	3.42		142	138
0.1	5.518	5.518	7.800	3.02			125	104
0.2	5.498	5.490	7.768	3.04			100	75
0.3	5.464	5.570	7.725	3.04	0.69	140		
0.4	5.436	5.546	7.701	3.04		190		
0.5	5.410	5.520	7.659	2.99	1.98	220	160	
0.6	5.399	5.502	7.625	3.01		280	165	
0.7	5.390	5.494	7.611	3.04	1.96		170	
0.8	5.359	5.466	7.577	3.03	1.94	265		
1.0	5.337	5.328	7.527	3.00	1.36	200	170[a]	

[a]As reported for nonstoichiometric $CaVO_3$ by Ref. 18.

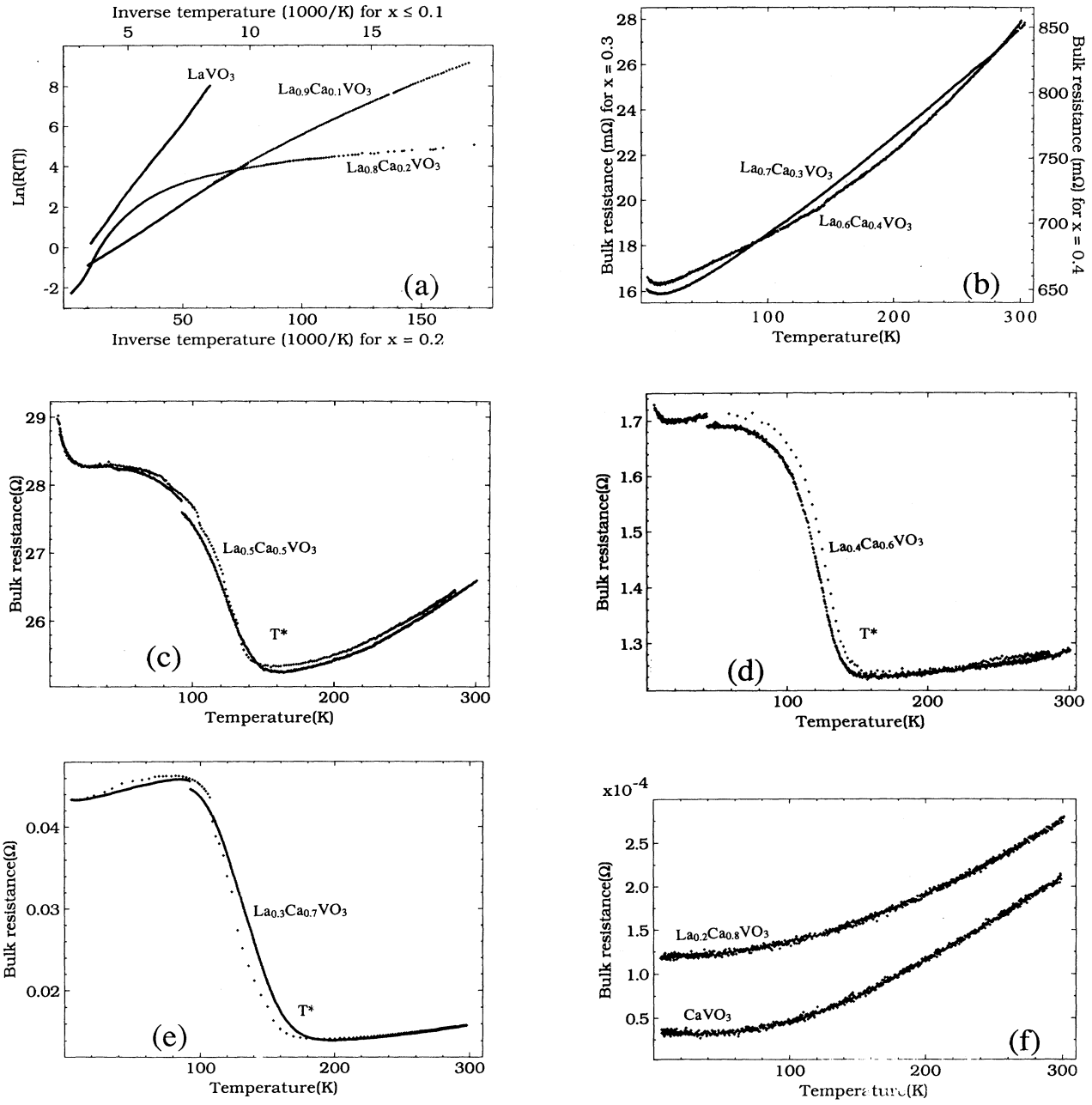

FIG. 2. (a) Ln (R) vs $1/T$ for $0 \leq x \leq 0.2$ for $La_{1-x}Ca_xVO_{3\pm\delta}$. (b)–(f) R vs T of $La_{1-x}Ca_xVO_{3\pm\delta}$ for $0.3 \leq x \leq 1.0$.

$0.3 < x \leq 0.7$. An apparent deviation from Végard's law (the dashed curve in Fig. 1) also appears in the range $0.5 < x \leq 0.7$. Table I gives the room-temperature lattice parameters and the oxygen parameters as determined by TGA.

(2) *Resistance and Seebeck data:* The four-probe dc resistance measurements made on cooling from room temperature to 4 K are summarized in Fig. 2; they reveal an *I-M* transition occurring in the range $0.2 < x < 0.3$, which confirms an $x_c \approx 0.26$ previously reported.[3] In the semiconductive range $0 \leq x \leq 0.2$, the extrinsic conduction at low temperatures increases systematically with x, and the small activation energies decrease with increasing x as reported previously.[3]

The change from a semiconductive $R(T)$ for $x = 0.2$ to a metallic $R(T)$ for $x = 0.3$ is quite dramatic. For $x = 0.3$ and 0.4, the temperature dependence of the resistance can be fit to the relation

$$R(T) \sim R_0 + a_{e\text{-ph}}T + a_{e\text{-}e}T^2 , \tag{2}$$

where $a_{e\text{-ph}}$ and $a_{e\text{-}e}$, respectively, are coefficients for

TABLE II. The curve-fitting parameters for $R(T)=R_0+a_{e\text{-ph}}T+a_{e-e}T^2$ from resistance data in Fig. 2 for $La_{1-x}Ca_xVO_3$ with $0\le x\le 1$.

$x=$	R_0 (Ω)	$a_{e\text{-ph}}$ ($\Omega\,K^2$)	a_{e-e} ($\Omega\,K^2$)	Range of fitting temperature
0.3	1.6×10^{-2}	2.6×10^{-5}	5.0×10^{-8}	whole curve
0.4	6.5×10^{-1}	2.3×10^{-4}	1.5×10^{-6}	whole curve
0.5	$2.4\times10^{+1}$	5.7×10^{-4}	2.4×10^{-5}	$T>250$ K
0.6	1.1×10^{0}	4.6×10^{-5}	≈0	$T>250$ K
0.7	9.2×10^{-3}	2.2×10^{-5}	≈0	$T>250$ K
0.8	1.2×10^{-4}	2.0×10^{-9}	1.8×10^{-9}	whole curve
1.0	3.2×10^{-5}	≈0	2.2×10^{-9}	whole curve

electron-phonon and electron-electron interactions of a strongly correlated Fermi liquid. The measured parameters are given in Table II. A similar curve fitting is possible for samples $x=0.8$ and 1.0; for $CaVO_3$, an $R(T)\sim T^2$ dependence shows a resistance completely dominated by electron-electron interactions. However, in the intermediate range $0.5\le x\le 0.7$ this T^2 behavior is only found above 160 K; an anomalous step in the resistance is found at lower temperatures, $T<T^*$.

The Seebeck coefficients $S(T)$ obtained on cooling from room temperature to 20 K are summarized in Fig. 3. The curve for $x=0.1$, Fig. 3(a), is representative of the semiconductive samples; an $S>0$ increases abruptly on cooling through the Néel temperature $T_N\approx125$ K. In the temperature range $T>T_N$, $S(T)\sim E_a/kT$ varies as for a semiconductor; a measured E_a smaller than that obtained from the $R(T)$ curve was found, which indicates small-polaron conduction of the intrinsic charge carriers as was also reported earlier.[3] An increase of the activation energy E_a for creation of mobile charge carriers occurs on cooling through T_N. Below 40 K, the mobile carriers of positive charge become frozen out; $S(T)$ becomes negative at lowest temperatures.

In the metallic samples, the Seebeck data for the compositions $0.5\le x\le 0.7$ remain positive, whereas the $x=0.3$ and 0.4 samples have an $S<0$ in the range $40<T<180$ K, and $CaVO_3$ has an $S<0$ for all temperatures. The $x=0.8$ sample appears to be transitional in character.

(3) *Magnetic data:* The molar susceptibility $\chi_m(T)=M/H$ was measured while heating in a field $H=1$ kOe after the sample was cooled in either zero field, the case (ZFC), or in a field of 1 kOe applied in the same direction as the measuring field, the FC-1-kOe case. The results are given in Figs. 4 and 5.

Comparison of the ZFC and FC-1-kOe curves for $x=0$, 0.1, and 0.2 is shown in Figs. 4(a) and 4(b). Long-range magnetic order is evident below a Néel temperature T_N; it gives a canted-spin configuration having a ferromagnetic component. Cooling in zero field leaves the sample demagnetized, but cooling in 1 kOe initially favors magnetic domains having a component of their magnetization aligned in the direction of the applied field. Consequently $\chi_m(T)$ increases abruptly on cooling through T_N, however, for $x=0$ and 0.1, it reverses sign on cooling through $T_t<T_N$. The sign reversal is reversible on heating through T_t. A large magnetocrystalline anisotropy prevents the initiation of reversible domain-wall motion below T_N in 1 kOe, so the ZFC curve is like that of a typical antiferromagnet.

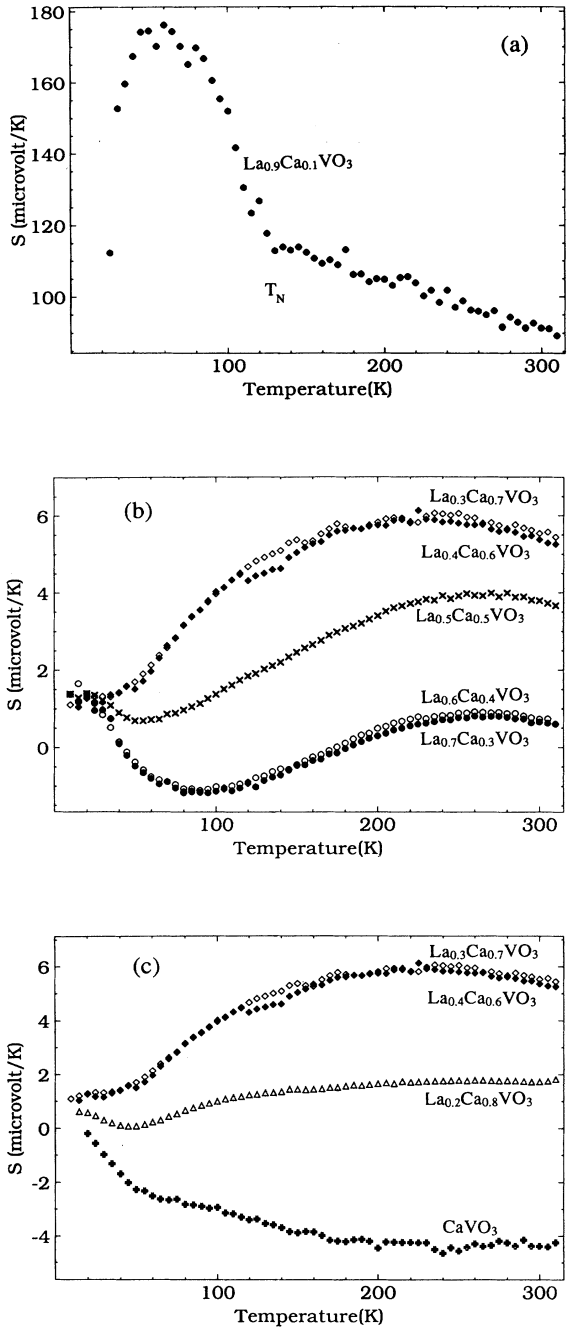

FIG. 3. Seebeck coefficient vs temperature of $La_{1-x}Ca_xVO_{3\pm\delta}$ for (a) $x=0.1$, (b) $0.3\le x\le 0.7$, and (c) $0.6\le x\le 1.0$.

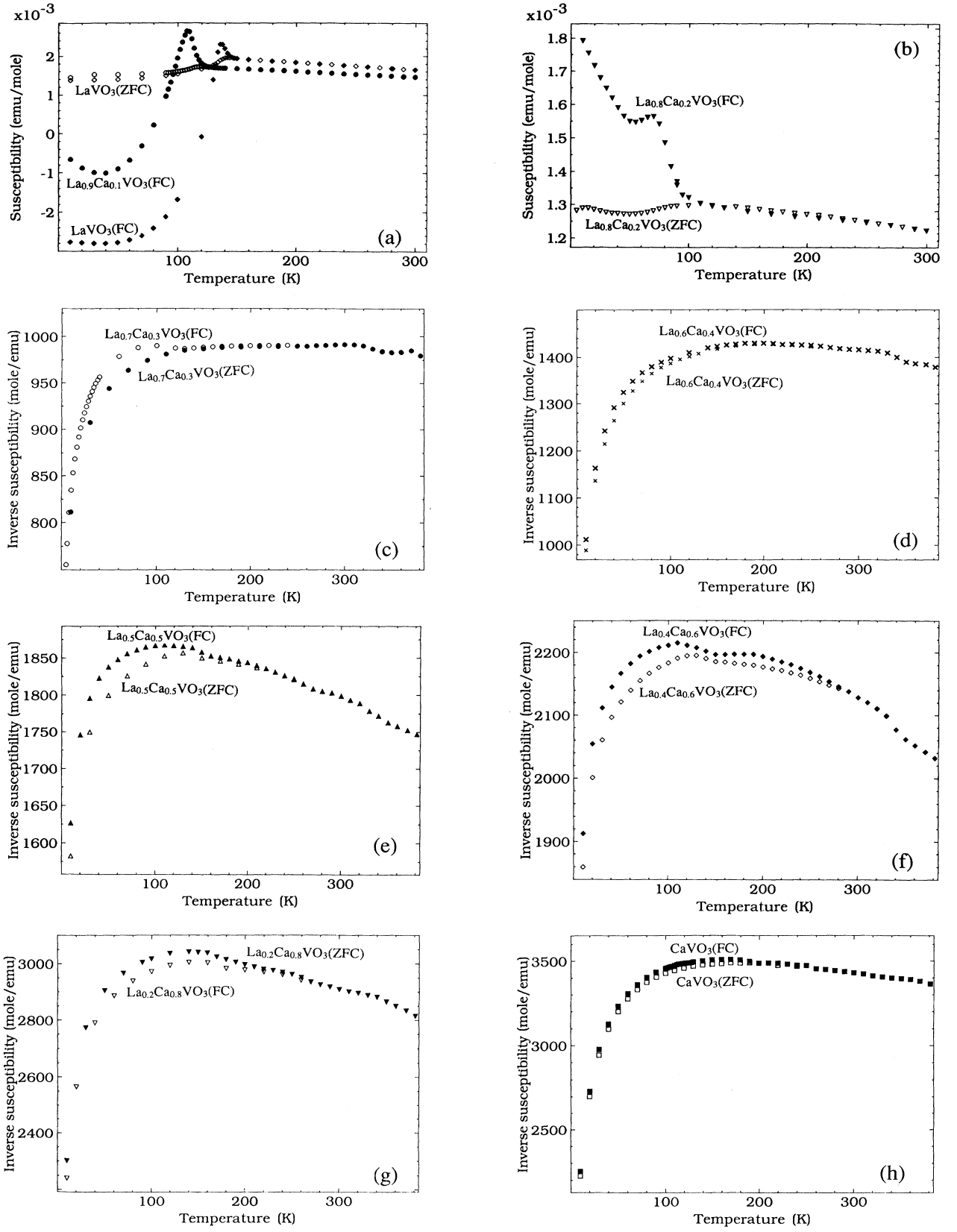

FIG. 4. Magnetic susceptibility ($H = 1$ kOe) vs temperature for (a) $x \leq 0.1$ and (b) $x = 0.2$ for $La_{1-x}Ca_xVO_{3\pm\delta}$. (c)–(h) Inverse molar magnetic susceptibility ($H = 1$ kOe) vs temperature of $La_{1-x}Ca_xVO_{3\pm\delta}$ for $0.3 \leq x \leq 1.0$.

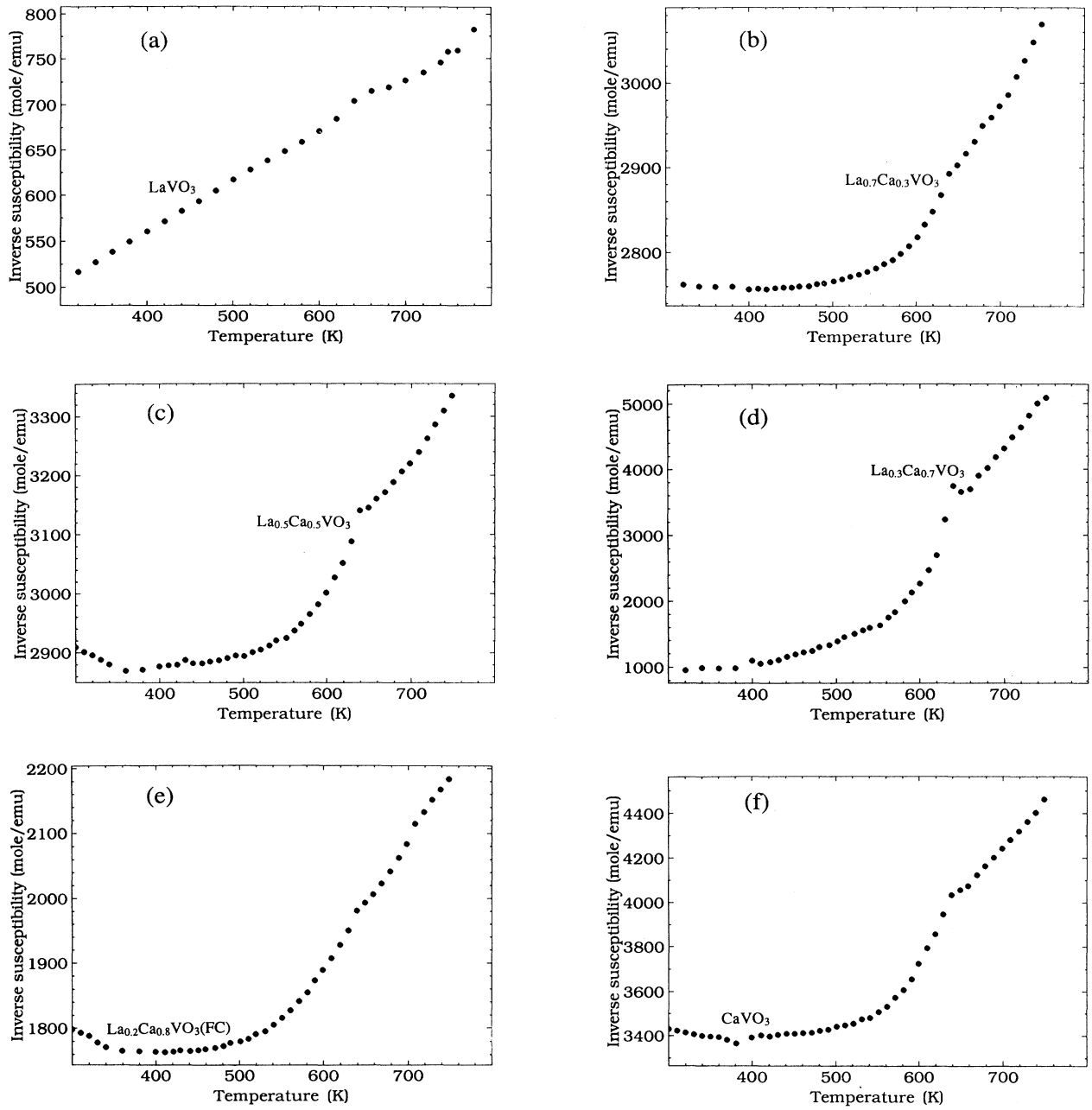

FIG. 5. Inverse molar magnetic susceptibility ($H=1$ kOe) vs temperature of $La_{1-x}Ca_xVO_{3\pm\delta}$ for $x=0$, 0.3, 0.5, 0.7, 0.8, and 1.0.

Reversal of the magnetization of the $x=0$ and 0.1 samples marks a first-order magnetostrictive distortion occurring below T_t; the vanadium magnetic moments apparently change sign on thermally traversing T_t, as has been systematically demonstrated elsewhere.[12,13] The origin of this phenomenon is a discontinuous change in the orbital angular momentum on traversing T_t. The Néel temperature T_N decreases from 142 K for $x=0$ to 125 K for $x=0.1$ to 100 K for $x=0.2$; the magnetostrictive onset temperature T_t decreases with decreasing V^{3+}-ion concentration from 138 K for $x=0$ to 104 K for $x=0.1$ and 75 K for $x=0.2$. In the $x=0.2$ sample, the difference $T_N-T_t\approx 25$ K appears to be too great for the change in orbital angular momentum at T_t to reverse the sign of the magnetization in opposition to the coupling of the field to the spin component of the atomic moments; the anomaly at T_t in this sample appears to reflect only a large increase in the magnetocrystalline anisotropy on traversing T_t.

Whereas Mahajan *et al.*[5] found only Pauli paramagne-

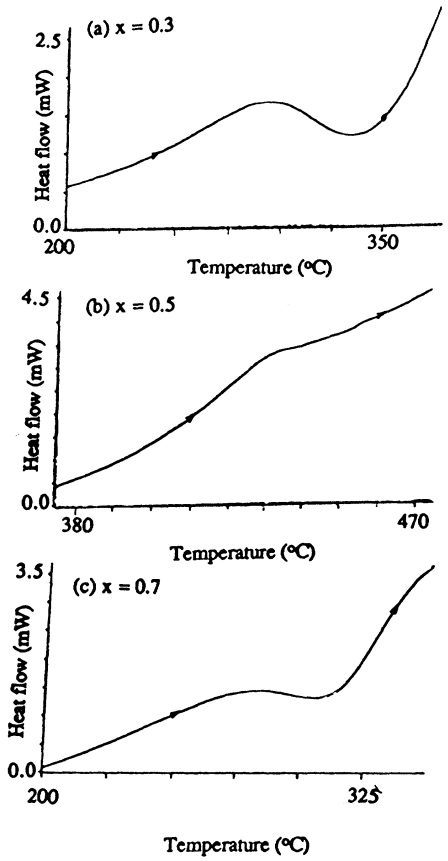

FIG. 6. Heat flow obtained with DSC vs temperature taken on heating at 10°/min for $La_{1-x}Ca_xVO_{3\pm\delta}$: (a) $x=0.3$, (b) $x=0.5$, and (c) $x=0.7$.

tism below 400 K for all $x>x_c$ in $La_{1-x}Sr_xVO_3$, the data of Fig. 4 show a weak divergence of the ZFC and FC-1-kOe curves below 300 K for $x\geq 0.3$ in $La_{1-x}Ca_xVO_3$. This divergence is evidence for a spin-blocking temperature T_{sg} that increases monotonically from 140 K for $x=0.3$ to a maximum of 280 K at $x=0.6$, decreasing to 265 K at $x=0.8$. All samples $0.3\leq x\leq 1$ show an increase in $\chi_m(T)$ with decreasing T below 100 K; this increase is indicative of paramagnetic localized spins associated with defects, chemical inhomogeneities, and/or surface vanadium.

The $(\chi_m)^{-1}$ vs T curves shown in Fig. 5 were taken in vacuum; the composition should not change under these conditions. Differential scanning calorimetry (Fig. 6) indicates that a first-order phase change occurs in the range 320–420 °C, with a maximum at $x=0.5$, where the susceptibility shows an anomaly. The heating curves (Fig. 5) were reproducible after cooling to room temperature, but a large thermal hysteresis in the susceptibility was observed on cooling. The high-temperature phase exhibits a Curie-Weiss law typical of some localized spins with a small Pauli-paramagnetic background, whereas the low-temperature phase exhibits an enhanced Pauli paramagnetism below 500 K with evidence of some type of magnetic order below 280 K. The fact that the transition temperature near 640 K is evident even in $LaVO_3$, and remains nearly constant for all x, indicates that it is structurally driven; it is probably an orthorhombic-cubic transition.

DISCUSSION

Stoichiometric $LaVO_3$ is an insulator with the occupied V^{4+}/V^{3+} couple lying above the top of the predominantly $O^{2-}:2p^6$ valence band; the empty V^{3+}/V^{2+} couple remains below the bottom of the V 4s conduction band, but it is split from the V^{4+}/V^{3+} couple by the on-site electrostatic Coulomb energy commonly referred to as the Hubbard U [Fig. 7(a)]. In an ionic model, the empty V^{3+}/V^{2+} couple lies far enough above the top of the valence band that covalent mixing of V 3d and O 2p orbitals can be treated in second-order perturbation theory within the context of a localized ligand-field theory; the resulting localized $^3T_{1g}$ configuration for the $V^{3+}:t^2e^0$ configuration in an octahedral site describes well the physical properties observed. In a cubic field, the orbital angular momentum is not completely quenched, and below T_t a local trigonal distortion with $\alpha>60°$ signals that the $m=\pm 1$ state is stabilized relative to the $m=0$ state at the V^{3+} ions.[11] This magnetostrictive distortion is responsible for the anomalous diamagnetism shown in Fig. 4(a).[12,13] It is only found where the $3d^n$ configuration

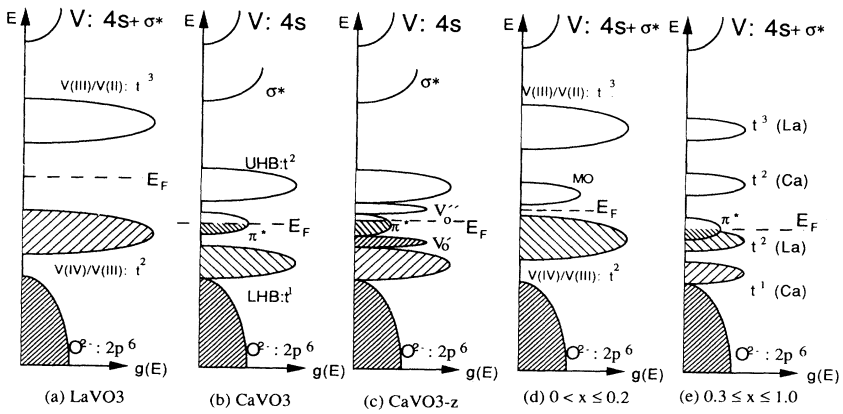

FIG. 7. Schematic energy diagram for (a) $LaVO_3$, (b) $CaVO_3$, (c) $CaVO_{2.97}$, (d) $0<x\leq 0.2$, and (e) $0.3\leq x\leq 1.0$ for $T>400$ K. V_O' is an oxygen vacancy with one trapped electron, V_O'' is a vacancy with two trapped electrons. In (e), (Ca) and (La) refer to states in the hole-rich and hole-poor domains, respectively.

is localized.

It should be noted that the compound YVO_3 shows no magnetostrictive distortion below T_N;[13] it appears to be an itinerant-electron antiferromagnet with strong correlations providing upper and lower Hubbard bands as pictured in Fig. 7(a) and also in Ref. 6. The distinction between the localized-electron antiferromagnetism of $LaVO_3$ and the itinerant-electron antiferromagnetism of YVO_3 is not captured in schematic energy diagrams like Fig. 7(a). The observation[13] that a pressure greater than 8 kbar can induce a first-order transition in $LaVO_3$ to a delocalized, though still strongly correlated, antiferromagnetic state with a shorter equilibrium V—O bond length indicates that a ligand-field description with nearest-neighbor interatomic interactions treated in second-order perturbation theory is only just applicable to the $(VO_3)^{3-}$ array.

Oxidation of the $(VO_3)^{3-}$ array to $(VO_3)^{2-}$ by substitution of La^{3+} by Sr^{2+} or Ca^{2+} lowers by U the energy required to transfer an electron from an O $2p$ to an empty V $3d$ orbital, which increases the covalent mixing and therefore the interatomic electron-transfer integrals for the V-O interaction and for the V-O-V interactions.[1] Consequently $CaVO_3$ and $SrVO_3$ have, at least at and below room temperature, some itinerant electrons in a narrow π^* band of t-orbital parentage. The electron-electron interactions remain dominant in the narrow π^* band, and the single-valent stoichiometric composition manifests an on-site electron-electron interaction $U < W_\pi$, which makes the compound an exchange-enhanced, Pauli-paramagnetic metal. According to Kotliar, Rozenberg, and Zhang,[23] we can expect to find the coexistence of Hubbard bands and a narrow π^* Fermi-liquid band at the crossover from antiferromagnetism to Pauli paramagnetism as is illustrated in Fig. 7(b).

Loss of oxygen from $CaVO_3$ reduces the $VO_{3-\delta}$ array and perturbs the periodic potential energy of the electrons. One of the two electrons per oxygen vacancy becomes trapped as a localized spin-$\frac{1}{2}$ state at the vacancy; the second electron appears to be donated to the π^* band since the trapped electrons contribute a Curie-Weiss term to $\chi_m(T)$ (Ref. 19) and apparently couple to one another via the metallic π^* electrons below a spin-blocking temperature $T_{sg} \approx 200$ K [Fig. 4(h)]. Figure 7(c) illustrates schematically the density of electronic states versus energy for $CaVO_{3-\delta}$. Localized spins may also reside on V^{3+} ions neighboring an oxygen vacancy.

Initial oxidation of the VO_3 array by substitution of Ca^{2+} for Ln^{3+} in the system $La_{1-x}Ca_xVO_3$ introduces holes into the localized V(IV)/V(III) couple of Fig. 7(a) to give the modified energy diagram of Fig. 7(d). Electrostatic forces tend to trap the holes at the eight vanadium atoms near neighbor to a Ca^{2+} ion. Holes excited from the trap apparently form small-polaron charge carriers in the hole-poor regions, and long-range antiferromagnetic order introduces an added intraatomic-exchange energy to the local-deformation barrier to hole migration. We attribute the curvature in the $\ln R(T)$ vs $1/T$ plot for $La_{0.9}Ca_{0.1}VO_3$ in Fig. 2(a) to the gradual increase in the motional enthalpy ΔH_m of the small polarons with increasing magnetic order; the more abrupt jump in $S(T)$ vs T [Fig. 3(a)] reflects suppression below T_N of the spin-degeneracy term $\beta=2$ in the small-polaron statistical contribution to the Seebeck coefficient:

$$S=(k/e)\ln[\beta(1-c)/c] , \tag{3}$$

where c is the fraction of vanadium sites occupied by mobile holes. The temperature dependence of S for $T > T_N$ reflects a temperature-dependent fraction $c(T)$, which makes the activation energy E_A obtained from $S(T)$ for $T > T_N$ a measure of the trapping energy ΔH_t of the hole by the Ca^{2+} ions: $E_A = \Delta H_t/2$. The difference in the activation energy $E_g/2$ obtained from the $\ln R$ vs $1/T$ plot and E_A would normally give the motional enthalpy of the polaron:

$$\Delta H_m = (E_g - \Delta H_t)/2 . \tag{4}$$

However, both E_g and ΔH_m decrease as the Ca^{2+}-ion concentration approaches the percolation threshold. Therefore, these changes appear to be due to a lowering of the energy for hopping between clusters as the percolation threshold is approached, which implies a transition to a variable-range hopping as x increases toward x_c.

The small-polaron character applies only to the mobile holes excited to the antiferromagnetic matrix out of the eight vanadium trap sites near neighbor to a Ca^{2+} ion. Small polarons move too slowly to couple neighboring spins ferromagnetically via the double-exchange mechanism,[1] so the matrix remains antiferromagnetic with a T_N that decreases only gradually with increasing x. Since the eight vanadium trap sites near neighbor to a Ca^{2+} ion do not become superparamagnetic, a ferromagnetic superexchange mechanism must not be operative within the clusters despite the higher hole fraction on the vanadium atoms of a cluster. We conclude, therefore, that the holes either remain polaronic within a cluster or transform the cluster orbitals from localized to molecular-orbital (MO) states. The abrupt transition to a metallic, mostly Pauli paramagnetic behavior at a percolation threshold $x_c \approx 0.26$, seems more consistent with the formation of MO states in the eight vandium clusters. An abrupt shortening of the mean V-O distance and straightening of the V—O—V bond angle would distinguish the MO phase within a cluster from the localized-electron phase of the antiferromagnetic matrix. Hopping between clusters as x approaches x_c would be analogous to variable-range hopping.

The evolution with x of the electronic properties of $La_{1-x}Ca_xVO_3$ is in contrast with that of $La_{1-x}Ca_xMnO_3$.[24,25] In both systems there is a transition from localized electrons in the antiferromagnetic insulators $LaVO_3$ and $LaMnO_3$, each of which exhibits a cooperative Jahn-Teller distortion at lower temperatures, to itinerant-electron behavior with increasing x. However, $La_{1-x}Ca_xMnO_3$ becomes a metallic ferromagnet via double exchange for $x > x_c$, whereas $La_{1-x}Ca_xVO_3$ becomes a Pauli paramagnetic metal. In $La_{1-x}Ca_xMnO_3$,

the transition from localized to itinerant electrons occurs only for the σ-bonding electrons of e-orbital parentage at the high-spin manganese ions: Mn(IV):$t^3e^1 \rightarrow$Mn(IV/III):$t^3\sigma^{*(1-x)}$. In $La_{1-x}Ca_xVO_3$, on the other hand, the V(III): $t^2 \rightarrow$V(IV/III):$\pi^{*(2-x)}$ transition leaves no localized electrons on the vanadium atoms, so the transition from localized to itinerant electrons is from an antiferromagnetic-insulator parent phase to a metallic phase without long-range magnetic order.

Extrapolation of this model to beyond the percolation threshold at $x_c \approx 0.26$ gives the energy diagram of Fig. 7(e) for stoichiometric compositions below 300 K. As the MO states of the isolated clusters of vanadium atoms near neighbor to a Ca^{2+} ion are transformed into extended narrow-π^*-band states, pockets of the localized-electron phase would be retained; localized states of the associated upper and lower Hubbard bands remain split by the energy U, as is also indicated in Fig. 7(e). The localized-state domains would order antiferromagnetically below T_N and, in FC-1-kOe samples, introduce an important contribution to the magnetic susceptibility. This contribution is evident in Figs. 4(c)–4(g). On the other hand, metallic conduction occurs in the itinerant-electron states of the hole-rich phase; the extended states of this phase are derived from spectral weight that is transferred from both the upper and lower Hubbard bands. In addition, retention of Hubbard-band states even in $CaVO_3$, Fig. 7(b), indicates that "correlation fluctuations" exist within the Fermi-liquid domains to contribute additional Hubbard states. There may also be an additional contribution to the localized spins from vanadium atoms near lattice defects in the metallic phase. The Fermi energy E_F must fall below any mobility edge μ_c within the π^* bands; localized spins associated with atomic vacancies or lattice defects are not shown.

In the interval $0.5 \leq x \leq 0.7$, a step in the resistance occurs below a $T^* \approx T_N$, where T_N is the Néel temperature of the localized-electron, hole-poor phase. The absence of this step in the $x = 0.3$ and 0.4 samples is, therefore, surprising. $T^* \approx T_N$ suggests that the step is associated with the stabilization of long-range magnetic order in the hole-poor phase that induces a spin-density wave in the metallic phase. Since the deviation from Végard's law noted in Fig. 1 in the interval $0.6 \leq x \leq 0.8$ overlaps the interval where a step in $R(T)$ is observed, we suspect the presence of chemical inhomogeneities due to the initiation of a phase segregation into Ca-rich and Ca-poor perovskite regions at lower temperatures in the interval $0.5 \leq x \leq 0.8$; the segregation does not reach equilibrium during cooling from the firing temperature in our samples, so two perovskite phases of different lattice parameters are not detected in the x-ray powder-diffraction patterns. However, the introduction of chemical inhomogeneities by initiation of a spinodal phase segregation could give a long-range magnetic ordering within the hole-poor domains.

The I-M transition at x_c is marked by a dramatic drop in the magnitude of the Seebeck coefficient. The only metallic samples that retain an $S > 0$ for all $T < 300$ K fall in the range $0.5 \leq x \leq 0.7$, where a T^* is found. However, $S(T)$ shows no anomaly near T^*, only a smooth increase in S. Below 300 K, the broad maximum in $S(T)$ in the range $0.5 \leq x \leq 0.7$ appears to correlate with the spin-blocking temperature T_{sg}, which in turn is expected to be sensitive to oxygen stoichiometry and lattice defects. The system behaves as though fluctuations of the localized spins at defects within the metallic phase give rise to a positive spin enhancement of the Seebeck coefficient that has its maximum value where the concentration of localized spins is greatest. In our $CaVO_3$ sample, there is no evidence of any spin enhancement; the Seebeck coefficient remains negative for all $T < 300$ K.

A negative Seebeck coefficient for the $x = 0.3$ and 0.4 samples at low temperatures is consistent with a trapping of holes in a π^* band of a percolating phase. A positive enhancement factor due to the presence of localized spins could drive $S(T)$ positive at its maximum values near T_{sg}.

At higher temperatures $400 < T < 640$ K, the $[\chi_m(T)]^{-1}$ curves for the metallic samples of Fig. 5 become temperature dependent and exhibit a thermal hysteresis; the structural phase change near 640 K on heating is clearly first order, and the high-temperature phase contains localized spins.

Finally, we turn to the evolution with x of the unit-cell volume, Fig. 1. A discontinuous increase in volume occurs on increasing x through the I-M transition at x_c. With a global electronic model in the mixed-valent system $La_{1-x}Ca_xVO_3$, we would predict a shortening of the mean V—O bond length on going from the localized to the itinerant electronic regime, as is observed[26] in $NdNiO_3$; however, we seem to observe a small increase in the lattice parameter. On the other hand, if the initial holes trapped at Ca^{2+} ions already occupy MO states to give an effective electronic phase separation into MO and localized electronic states, then the evolution of the volume and lattice parameters with x may only reflect the atomic solid solution; in this case, the single unit-cell volume obtained from room-temperature powder x-ray diffraction would vary linearly with x in accordance with Végard's law over the entire compositional range $0 \leq x \leq 1$. An electronic phase segregation induced by oxygen displacement would have too small an effect on the local lattice parameters to be easily detected by powder x-ray diffraction, particularly at room temperature where excitation of holes to the hole-poor phase tends to reduce the distinction between mean V—O bond lengths in the two phases. At higher temperatures, a transition to a single, global electronic phase can be anticipated.

Previous workers have observed that Végard's law appears to be obeyed at room temperature for both the $La_{1-x}Ca_xVO_3$ (Ref. 3) and $La_{1-x}Sr_xVO_3$ (Refs. 4 and 5) systems. In fact, the deviations from Végard's law that are suggested by the dashed line in Fig. 1 and the break in Végard's law at the I-M transition are small, and may reflect only changes in the mean V—O—V bond angles on going from O' to O orthorhombic symmetry. In addition, room-temperature ^{51}V NMR data show no evidence of antiferromagnetic spin fluctuations in the metallic samples of $La_{1-x}Sr_xVO_3$, which indicates a global metallic phase at room temperature in this system. Also, an apparent abrupt disappearance of long-range magnetic

order at x_c would seem to argue that any localized-electron phase fails to percolate through the samples. Nevertheless, magnetic-susceptibility data [Figs. 4(c)–4(g)] show evidence of antiferromagnetic order below 140 K in at least a part of the sample; in samples $0.5 \leq x \leq 0.7$ a step also occurs in the resistance below $T^* \approx 140$ K, indicative of a long-range magnetic ordering in the metallic phase as well. We contend that the available structural data for $La_{1-x}Ca_xVO_3$ are consistent with two electronic phases within an atomically single-phase region, provided the two electronic phases are segregated by cooperative oxygen-atom displacements occurring below 400 K.

In the system $Y_{1-x}Ca_xVO_3$, on the other hand, bond-length mismatch in the end member YVO_3 places the V—O bonds under greater compression than in $LaVO_3$, which transforms the localized t_2 electrons of $LaVO_3$ into narrow-π^*-band electrons in YVO_3. However, a greater deviation of the V—O—V bond angle from 180° in YVO_3 keeps the π^* bands narrow with strong electron correlations; YVO_3 is an antiferromagnetic insulator although without a magnetostrictive distortion below T_N. In this system, substitution of Ca^{2+} for Y^{3+} does not appear to trap holes in MO states, but as small polarons at Ca^{2+} ions. As a result, the threshold of interest is not the percolation threshold for V atoms near neighbor to Ca^{2+} ions, but the composition at which a change from polaronic to itinerant mobile holes introduces a change in their kinetic energy $\langle T \rangle$, which would be manifest in a contraction of the lattice according to the Virial theorem. The discontinuous step in the evolution of the unit-cell volume with x at an $x_c \approx 0.75$ (see Fig. 1) would suggest a first-order phase change from polaronic to itinerant-electron behavior.

CONCLUSIONS

Although powder x-ray diffraction indicates a continuous atomic solid solution over the entire compositional range $0 \leq x \leq 1$ of the perovskite system $La_{1-x}Ca_xVO_3$, the absence of a volume contraction at x_c or of a ferromagnetic double-exchange interaction for any value of x indicates that no global change from localized-electron to itinerant-electron behavior occurs at the *I-M* transition at $x_c \approx 0.26$. Magnetic and transport data below 300 K support a model in which two distinguishable electronic phases are present below 300 K. Failure to observe two distinguishable crystallographic phases is attributed to an electron phase segregation driven only by oxygen-atom displacements. This process is believed to commence at small values of x by the formation of eight vanadium MO cluster states about isolated Ca^{2+} ions. Formation of extended itinerant-electron states occurs at the percolation threshold $x_c \approx 0.26$. The lack of any evidence for a ferromagnetic double-exchange interaction is attributed to a first-order transition from localized to itinerant electronic behavior in the partially occupied π^* band. Double-exchange ferromagnetism occurs in the system $La_{1-x}Ca_xMnO_3$ because the localized-itinerant electron-

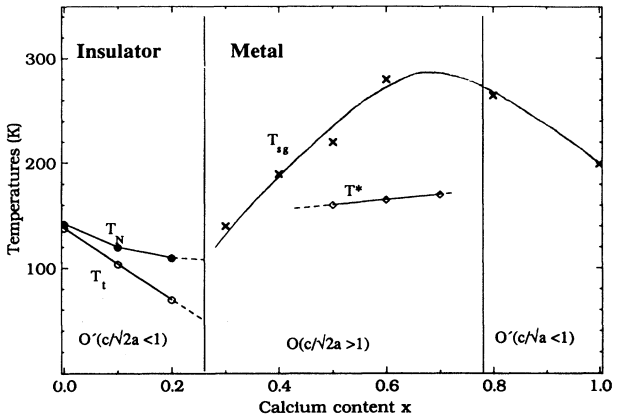

FIG. 8. Preliminary phase diagram for $La_{1-x}Ca_xVO_{3\pm\delta}$, $0 \leq x \leq 1$. Solid lines are drawn for guides to the eye.

ic transition occurs only for σ-bonding electrons in the presence of a localized t^3 configuration. For small hole concentrations, the first-order t-π^* transition in $La_{1-x}Ca_xVO_3$ traps holes in MO states at Ca^{2+} ions while introducing small-polaron excited holes to the localized-electron matrix. A transition to variable-range hopping occurs rather than a transition from small-polaron to itinerant-electron behavior in the hole-poor regions. This behavior contrasts with that of $Y_{1-x}Ca_xVO_3$.

Analysis of our data leads to the phase diagram of Fig. 8. The several critical parameters are as follows.

(a) T_N is the Néel temperature below which long-range antiferromagnetic order occurs with a canted-spin ferromagnetism; as x approaches x_c, individual vanadium atoms begin to have more than one Ca neighbor, so the number of magnetic vanadium removed per Ca^{2+} ion decreases and dT_N/dx takes a shallower slope.

(b) T_t is the localized electron magnetostrictive distortion associated with localized ${}^3T_{1g}$ configurations at V^{3+} ions; it disappears with the long-range magnetic ordering below a T_N as x crosses x_c.

(c) x_c is the percolation threshold at which the *I-M* transition occurs.

(d) x_d is the critical Ca^{2+} concentration $0.1 < x_d < 0.2$ above which $T_N - T_t$ becomes too large to stabilize an anomalous diamagnetism in FC-1-kOe samples on cooling through T_t.

(e) T^* is a temperature marking the bottom of a step in the $R(T)$ curve; it appears to coincide with a T_N for the hole-poor domains in the VO_3 array.

(f) T_{sg} is the temperature below which free rotation of localized spins within the metallic phase are blocked; these localized spins are associated with atomic vacancies and/or lattice defects.

Not shown is the temperature interval 400–640 K of the nearly composition-independent hysteresis of a structural transition. A Curie-Weiss paramagnetism is found for $T > 640$ K.

Finally, we also note that the maximum in T_{sg} at $x \approx 0.7$ coincides with the maximum departure from

Végard's law to larger volume, which suggests that the defects responsible for the localized spins in the metallic phase and the small excess volume that is observed in the interval $0.5 \leq x \leq 0.8$ have a common origin and may be associated with the initiation of a spinodal phase segregation during cooling from a temperature of full solid solution.

Note added in proof. Photoemission spectroscopy data of Inoue *et al.*[27] show a coexistence of localized (Hubbard-band) states and Fermi-liquid (itinerant-electron) π^*-band states in the system $Sr_{1-x}Ca_xVO_3$ with a transfer of spectra weight from π^*-band to Hubbard-band states with increasing x.

ACKNOWLEDGMENTS

We thank the Robert A. Welch Foundation, Houston, Texas, the Texas Advanced Research Program, and the National Science Foundation for financial support.

[1]J. B. Goodenough, Prog. Solid State Chem. **5**, 145 (1972).
[2]P. Dougier, J. C. C. Fan, and J. B. Goodenough, J. Solid State Chem. **14**, 247 (1975).
[3]P. Dougier, D. Deglane, and P. Hagenmuller, J. Solid State Chem. **19**, 135 (1976).
[4]P. Dougier and P. Hagenmuller, J. Solid State Chem. **15**, 158 (1975).
[5]A. V. Mahajan, D. C. Johnston, D. R. Torgeson, and F. Borsa, Phys. Rev. B **46**, 10 973 (1994).
[6]M. Kasuya, Y. Tokura, T. Arima, H. Eisaki, and S. Uchida, Phys. Rev. B **47**, 6197 (1993).
[7]J. B. Goodenough and J. M. Longo, in *Crystallographic and Magnetic Properties of Perovskite and Related Compounds,* edited by K. H. Hellwege, Landolt-Börnstein, New Series, Group III, Vol. 14, Pt. a (Springer-Verlag, Berlin, 1970).
[8]D. B. Rogers, A. Ferretti, D. H. Ridgley, R. J. Arnott, and J. B. Goodenough, J. Appl. Phys. **37**, 1431 (1966).
[9]V. G. Zubkov, G. V. Gazuev, V. A. Perelyev, and G. P. Shveikeen, Fiz. Tverd. Tela (Leningrad) **15**, 1610 (1973) [Sov. Phys. Solid State **15**, 1079 (1973)].
[10]Q. Huang, A. Santoro, P. Bordet, M. Marezio, S. W. Cheong, and B. Battlogg (private communication).
[11]J. B. Goodenough, Phys. Rev. **171**, 466 (1968).
[12]H. C. Nguyen and J. B. Goodenough, C. R. Acad. Sci. Paris Ser. II **319**, 1285 (1994).
[13]H. C. Nguyen and J. B. Goodenough, Phys. Rev. B **52**, 324 (1995).
[14]N. Shirakawa and M. Ishikawa, Jpn. J. Appl. Phys. **30**, L755 (1991).
[15]A. V. Mahajan, D. C. Johnston, D. R. Torgeson, and F. Borsa, Physica C **185-189**, 1095 (1991).
[16]B. Reuter and M. Wollnik, Naturwissenchafen **50**, 569 (1963).
[17]B. L. Chamberland and P. S. Danielson, J. Solid State Chem. **3**, 243 (1971).
[18]F. Iga and Y. Nishihara, J. Phys. Soc. Jpn. **61**, 1867 (1992).
[19]A. Fukushima, F. Iga, H. I. Inoue, K. Murata, and Y. Nishihara, J. Phys. Soc. Jpn. **63**, 409 (1993).
[20]N. F. Mott, M. Pepper, S. Politt, R. M. Wallis, and C. J. Adkins, Proc. R. Soc. London Ser. A **345**, 169 (1975).
[21]R. G. Egdell, M. R. Harrison, M. D. Hills, L. Porte, and G. Wall, J. Phys. C **17**, 2889 (1984).
[22]J. B. Goodenough and J. Zhou, Phys. Rev. B **47**, 5275 (1993).
[23]M. J. Rozenberg, G. Kotliar, and X. Y. Zhang, Phys. Rev. B **49**, 10 181 (1994).
[24]G. H. Jonker and J. B. van Santen, Physica **16**, 337 (1950).
[25]C. Zener, Phys. Rev. **80**, 403 (1950).
[26]J. B. Torrance, P. Lacorre, A. I. Nazzal, E. J. Ansado, and Ch. Niederwayer, Phys. Rev. B **45**, 8209 (1992).
[27]I. H. Inoue *et al.*, Phys. Rev. Lett. **74**, 2539 (1995).